Journal of Water Process Engineering 66 (2024) 106039

Contents lists available at ScienceDirect

Journal of Water Process Engineering

journal homepage: www.elsevier.com/locate/jwpe

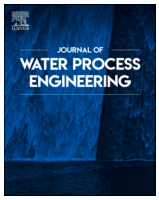

Effects of surfactants, ion valency and solution temperature on PFAS rejection in commercial reverse osmosis (RO) and nanofiltration (NF) processes

Qingquan Ma [a], Jiahe Zhang [a], Guangyu Zhu [a], Neel Ahuja [b], Boris Khusid [c], Wen Zhang [a,c,*]

[a] Department of Civil and Environmental Engineering, New Jersey Institute of Technology, Newark, NJ 07102, USA
[b] Millburn High School, Short Hills, NJ, USA
[c] Department of Chemical and Materials Engineering, New Jersey Institute of Technology, Newark, NJ 07102, USA

ARTICLE INFO

Editor: Ludovic F. Dumée

Keywords:
Reverse osmosis
Nanofiltration
PFAS
Membrane filtration
Rejection mechanisms

ABSTRACT

Per- and polyfluoroalkyl substances (PFAS) have garnered attention as a pressing environmental issue due to their enduring presence and suspected adverse health effects. This study assessed the rejection or removal efficacy of PFAS by commercial reverse osmosis (RO) and nanofiltration (NF) membranes and examined the impacts of surfactants, ion valency and solution temperature that are inadequately explored. The results reveal that the presence of cationic surfactants such as cetyltrimethylammonium bromide (CTAB) increased the rejection of two selected PFAS compounds, perfluorooctanoic acid (PFOA) and perfluorobutanoic acid (PFBA), by binding with negatively charged PFAS and preventing them from passing through membrane pores via size exclusion, whereas the presence of anionic surfactants such as sodium dodecyl sulfate (SDS) increased the PFAS rejection because the increased electrostatic repulsion prevented PFAS from approaching and adsorbing onto the membrane surface. Moreover, aqueous ions (e.g., Al^{3+} and PO_4^{3-}) with higher ion valency enabled higher rejection of PFOA and PFBA through increased effective molecular size and increased electronegativity. Finally, only high solution temperature at 45 °C significantly reduced PFAS rejection efficiency because of the thermally expanded membrane pores and thus the increased leakage of PFAS. Overall, this research provides valuable insights into the various factors impacting PFAS rejection in commercial RO and NF processes. These findings are crucial for developing efficient PFAS removal methods and optimizing existing treatment systems, thereby contributing significantly to the ongoing efforts to combat PFAS contamination.

1. Introduction

Per- and polyfluoroalkyl substances (PFAS), broadly utilized in various industrial and consumer applications [1], have emerged as a major concern because of their indefatigability, bioaccumulative nature, and negative consequences on human health and the environment [2]. Contamination of water sources by PFAS exacerbates these issues, demanding effective filtration and degradation methods for their removal. On April 10, 2024, EPA announced the final National Primary Drinking Water Regulation (NPDWR) establishing legally enforceable levels, called Maximum Contaminant Level (MCL) for PFOS and PFOA at 4 ng·L^{-1}, for PFNA, PFHxS, GenX at 10 ng·L^{-1}, and for mixture containing two or more of PFHxS, PFNA, GenX, and PFBS at 1 ng·L^{-1} in drinking water. These regulations have extended beyond the US, as governments worldwide have placed heavy restrictions on the two most common PFAS, PFOA and PFOS (8 carbon long-chain PFAS). Ascribed to the trace levels and prevalence of PFAS, elimination of PFAS from water/wastewater is still a formidable obstacle.

Various PFAS-removing techniques and technologies have been previously investigated, adsorption (e.g., activated carbon) and ion exchange (IX) resins are among the few commercially applied technologies by water treatment plants for removing PFAS [3]. Adsorption using powdered activated carbon (PAC) and granular activated carbon (GAC), which have shown effectiveness (e.g., >80 %) in removing long-chain PFAS (≥ 6 carbons) from water systems [4,5]. However, activated carbon techniques still struggle with the adsorption of short-chain PFAS (< 6 carbons) that have lower removal efficiencies of <40 % [6,7]. Moreover, dissolved organic carbon (DOC) in water could reduce the capacity

* Corresponding author at: Department of Civil and Environmental Engineering, New Jersey Institute of Technology, Newark, NJ 07102, USA.
E-mail address: wen.zhang@njit.edu (W. Zhang).

https://doi.org/10.1016/j.jwpe.2024.106039
Received 23 June 2024; Received in revised form 15 August 2024; Accepted 20 August 2024
Available online 31 August 2024

of GAC for PFAS removal and promote desorption, or decreased removal of PFAS as indicated by the release of PFAS previously adsorbed onto GAC [8,9]. Similarly, anion exchange resins, where PFAS with negative charge bind with the positively charged functional groups within resin, have also shown promise in filtering PFAS in water systems [10]. The quaternary ammonium or dimethyl ethanol ammonium polyacrylic gel resins have proven the most effective for PFAS removal (e.g., >90 %) [9]. The adsorption capacity ranges from 19 to 1090 $mg{\cdot}g^{-1}$, depending on the resin type and water characteristics (e.g., pH) [11]. However, both activated carbon and ion exchange removal techniques suffer from competitive adsorption, low adsorption capacities or affinity toward specific PFAS (e.g., short-carbon ones), and costs due to frequent chemical regeneration to restore the adsorbent material or expensive disposal of the exhausted adsorbents [12]. For instance, exhausted resins require chemical regeneration using a salt or base mixed with methanol or ethanol and produces toxic wastewater for disposal [13].

Membrane-based separation process has widely been studied for the removal of PFAS. Our previous study summarized the relevant literature that explored the influences of PFAS's carbon chain length, water matrices such as pH, ionic strength and organic matters, and transmembrane pressure on the membrane rejection of PFAS [14]. For example, high transmembrane pressure could result in high water recovery, despite of the operational cost rise. However, this high pressure could compress the membrane structure and ultimately affect the permeability and solute separation. Yu et al. reported a decrease in PFAS removal from 97 % to 94.5 % when increasing the transmembrane pressure from 0.4 MPa to 1.2 MPa due to the elevated membrane fouling potential, membrane compaction or concentration polarization. By contrast, the changes of solution pH, salinity and organic matters may change membrane surface properties (e.g., hydrophobicity and surface potential) and ionization states of PFAS. For example, Zeng et al. reported an increase in PFAS removal of 80 % to 98 % when increasing pH from 3.3 to 7 (initial feed concentration of 500 $mg{\cdot}L^{-1}$) [15]. Hara-Yamamura et al. reported an increase in PFAS removal of 9 % to 91 % when increasing the salt rejection ratio of NaCl from 28 % to 52 % by exposing the membrane to the hypochlorite solution [16]. Moreover, NOM could deposit and then form a fouling layer on membrane surfaces, influencing porosity, shape, and surface states and hence PFAS retention [9,17]. Wang et al. claimed that PFOS bonded strongly to organic matters via hydrophobic interactions and slightly increased the PFOS rejection from 90 % to 93 % with bovine serum albumin (BSA) and >95 % with sodium alginate (SA) [17]. Clearly, the types of organic matters could exert different binding with membranes or even PFAS and result in changes of PFAS removal.

In addition to the above reported findings, there are still limited understandings of some chemical factors such as the valency of aqueous ions, surfactants and their types, and solution temperature variations that are present in complex wastewater or brines generated from industrial processes (e.g., mining and semiconductor manufacturing). The reported influences of common cations and anions in water on PFAS rejection in NF or RO filtration are largely debatable. For instance, Zhao et al. found that divalent cations such as Ca^{2+} and Mg^{2+} can bridge with the head functional groups of PFOS through electrostatic interactions [18], which may increase the apparent molecular weight of PFOS and the PFOS removal from 94.0 % (0.1 mM Ca^{2+}) to 99.3 % (1 mM Ca^{2+}) on the NF membrane due to the enhanced steric hindrance [18,19]. DFT analysis indicated that Na^{+} could only bind with one PFOS, whereas Ca^{2+} or Fe^{3+} preferred to coordinate with two PFOS molecules [20]. Conversely, Soriano et al. showed that cations may neutralize the negative charges on the NF/RO membrane surface and reduces electrostatic shielding effect, which negatively affects the PFAS removal [21]. Moreover, different anions (e.g., Cl^{-}, SO_4^{2-}, and PO_4^{3-}) may also affect membrane rejection of PFAS [20,22]. For instances, Zhao et al. proved that the presence of SO_4^{2-}, and PO_4^{3-} ions increased PFOS rejection rate of nanofiltration membrane from 92.65 % to 94.74 % and 97.60 %, respectively [20]. This increase could be ascribed to negatively charged anions that enhance the overall negativity on the NF membrane surface, increasing the electrostatic repulsion repelling the membrane and the negatively charged PFOS molecules. However, the same study also reported no significant change in PFOS rejection with the presence of Cl^{-} ions, highlighting how there is no definitive answer for the effect of anion presence on the impacts of PFAS by RO/NF processes.

Furthermore, surfactants are commonly present in wastewater due to the use of cleaning, detergents, emulsification, and foaming agents and even natural waters. Surfactants, amphiphilic molecules with both hydrophilic and hydrophobic regions, can interact with PFAS and affect their rejection during RO and NF filtration. Surfactants can compete with PFAS molecules for adsorption onto the surface of the RO or NF membrane. Depending on their relative affinities for the membrane surface, surfactants may either enhance or reduce the adsorption of PFAS. For example, cationic surfactants have positively charged hydrophilic heads and hydrophobic tails. These surfactants can interact with negatively charged PFAS due to electrostatic attraction and enhance the removal of some PFAS through coagulation, flocculation, or adsorption [23]. Particularly, among many surfactants, sodium dodecyl sulfate (SDS) and cetyltrimethylammonium bromide (CTAB) have been found to increase PFAS rejection by RO/NF membranes because surfactants can form micelles, which are aggregates of surfactant molecules in water [24,25]. CTAB and SDS are commonly utilized in industrial and consumer applications (e.g., household detergents, personal care products and antimicrobial agents) [26,27]. For example, Hara-Yamamura et al. reported an increase in PFPeS removal of 52 % to 96 % when increasing the molar ratio of a commercial surfactant Montaline™ C40 over PFAS from 0 to 7300 [16,28]. Anionic surfactants, similar to PFAS, have negatively charged hydrophilic heads and hydrophobic tails and may encounter PFAS for the active sites on membrane surface, which may increase or reduce the PFAS removal efficiency [23]. However, the effect of cationic surfactants on the PFAS removal via RO or NF is not well documented.

Similarly, the water temperature variations could have profound impacts on membrane properties such as porosity and rigidity and thus PFAS removal. Hang et al. reported that the PFAS removal decreased from 91 % to 85 % when increasing the feed solution temperature from 15 °C to 35 °C [29], due to the expanded the membrane pores that increased the passage of PFAS through the membrane. Das et al. reported that increasing solution temperatures from 50 °C to 70 °C led to a reduction of PFPeA rejection from 85 % to 58 % due to the thermal expansion of the NF polymer membrane, because of an increase in pore size, and thus, a reduction in PFAS pollutant rejection [30].

To further our understanding of the effects of the valency of common cations and anions, surfactants, and water temperature on PFAS rejection in RO/NF membrane process, this study systematically assessed the rejection of PFAS using commercial RO or NF membranes and synthetic water with variations of substance and temperature that mirrors complex PFAS-containing water such as brackish groundwater near coastal areas with seawater intrusion or chemical manufacturing effluent with high levels of specific cations and surfactants. Two different PFAS compounds, perfluorooctanoic acid (PFOA) and perfluorobutanoic acid (PFBA) with eight and four carbons respectively, were employed for comparative studies. Furthermore, the PFAS-spiked solutions mixed with different cationic and anionic ions (e.g., Na^{+}, Mg^{2+}, and Al^{3+}) at the same molar concentrations were used to compare the ion valency effect on PFAS removal. Similarly, different surfactants (e.g., CTAB and SDS) were further added to evaluate the interactions of surfactants and PFAS and the resulting PFAS rejection. The impact of solution temperature on membrane filtration and PFAS removal was assessed. Finally, the membrane surface characterization (e.g., PFAS accumulation and distribution) was examined through surface chemical and work function mapping by atomic force microscope (AFM).

2. Methods and materials

2.1. Membrane filtration unit preparation

The commercial RO membrane (BW30–2540) and NF membrane (NF90–2540), purchased from Dow FilmTec (Minneapolis, MN), both comprised a polyamide selective layer on the top membrane surface, a polysulfone intermediate layer, and a polyester support layer. A cross-flow membrane filtration device (Crossflow Cell CF042, Sterlitech, Kent, WA, USA) was assembled to host the membrane coupon with a filtration area of 42 cm^2. The detailed setup has been described in our previous study [14]. Briefly, a constant feed flow rate (30 $ml{\cdot}min^{-1}$) was maintained using a high performance liquid chromatography (HPLC) dual-head digital pump. Other relevant parameters such as solution salinity and temperature are described below.

2.2. PFAS rejection assessment

The two PFAS concentrations were measured by an Agilent Liquid Chromatography with tandem mass spectrometry (LC-MS-MS) [31]. The method detection limits (MDLs) for PFBA and PFOA are 47 $ng{\cdot}L^{-1}$ and 17 $ng{\cdot}L^{-1}$ respectively. The assessment experiments were conducted with the following factors, including different levels of surfactants (SDS and CTAB), different cationic and anionic ion types, and different feed solution temperatures. When varying these parameters, other parameters remained constant. For instance, a trans-membrane pressure of 55.0 bar and 13.8 bar was consistently used for RO and NF filtration, respectively. The resulting permeate flux of RO and NF membrane under 55 and 13.8 bar was 97 ± 0.3 LMH and 78 ± 1.8 LMH, respectively. An initial PFOA or PFBA concentration (10 $mg{\cdot}L^{-1}$) was consistently used in the following experiments The relatively high concentration of 10 mg L^{-1} for PFOA and PFBA was primarily used to facilitate effectively analytical measurement by the detection method as the residual PFAS concentration in the filtrate is usually low or even lower than the detection limit. To better assess the rejection and removal performance of the tested RO or NF systems, this study adopted a high concentration to effectively measure the remaining PFAS in the filtered water samples.

To investigate the impacts of the cationic and anionic surfactants' impacts on the PFAS rejection, the feed solution was spiked with SDS or CTAB to reach the final concentrations of 1 mM, 2 mM and 5 mM, separately. Similarly, other feed PFAS solutions were also prepared with sodium chloride (NaCl), magnesium chloride ($MgCl_2$), aluminum chloride ($AlCl_3$), sodium sulfate (Na_2SO_4) and sodium phosphate (Na_3PO_4) at the same molar concentration of 100 mM to evaluate the impacts from different cations or anions on PFAS rejection. For temperature effect experiments, the feed water temperature was maintained at 15, 25, 35 or 45 °C by being stored in a water bath (JOANLAB) and poured in a stirred cell (Sterlitech) just before experiments. Permeate and feed samples were collected after the system was equilibrated for 1 h at each condition. Removal rates or rejection of PFOA or PFBA by the RO and NF membranes under the above various conditions were determined accordingly by measuring the PFAS concentrations in the filtrate or permeate samples.

2.3. Chemical and electronic mapping of RO/NF membranes

The major methods for membrane properties such as permeability or pore size of the RO and NF membranes before and after filtration have thoroughly been characterized and reported in our previous study [14]. This study further employed AFM-IR to verify the changes of some other important membrane properties (e.g., surface chemical distribution and hydrophobicity). To examine the presence of PFAS adsorption on the membrane surface after filtration, a Bruker AFM-IR technology (NanoIR2, Anasys Instruments, Inc., Santa Barbara, CA, USA) was used in to map the membrane surfaces following our reported method [30,31].

To verify the PFAS adsorption on the RO/NF membrane surface after filtration, Kelvin probe force microscopy (KPFM) was further used to map the work function of the membrane surfaces following our reported method [32]. The work function arises from the electrostatic barrier created by the double dipole layer at the surface [33], which reflects the minimum energy required to move an electron from the interior of a solid material into the vacuum immediately adjacent to the surface of the material. The surface potential measured through KPFM corresponds to the contact potential difference (CPD), which represents the variation in work functions between the sample surface and the probe tip, as elaborated in Section S1 of the Supporting Information (SI).

2.4. Statistical analysis

The results (e.g., data points and bars) are represented by mean values ± standard deviation (SD) from duplicate or triplicate experiments. The differences between different test groups were tested using one-way analysis of variance (ANOVA) and post hoc *t*-test with significant difference at $p < 0.05$.

3. Results and discussions

3.1. Effects of cationic and anionic surfactants on PFOA and PFBA rejection

Fig. 1 compares the rejection of PFOA and PFBA in the presence of two different surfactants (SDS and CTAB) at three different concentrations (1 mM–5 mM). The rejection of PFOA or PFBA was both over 99 % for RO and higher than those for NF (Fig. 1a and b). As a result, neither SDS nor CTAB exerted any noticeable impacts on their rejections on RO. For the NF membrane, increasing the two surfactants' concentrations consistently enhanced both PFOA and PFBA rejection efficiency as presented in Fig. 1c and d, probably due to several different mechanisms. First, the surface accumulation of SDS or CTAB surfactants lowered the membrane permeate flux as shown in Tables S1 and S2. This fouled NF membrane could block or slow down the passage of PFAS. Secondly, the positively charged CTAB may bind with the negatively charged PFAS and form a complex cluster with large molecular sizes and thus enhance the rejection. By comparison, the negatively charged SDS would likely conquer the surface adsorption sites and increase negative charges on membrane surface, which have been confirmed with surface zeta potential data in Fig. S3 and improved the PFAS rejection.

3.2. Effects of ion valence on PFOA and PFBA rejection

Surface and groundwater always include common ions such as aluminum (Al^{3+}), calcium (Ca^{2+}), magnesium (Mg^{2+}), and sodium (Na^{+}), or typical anions such as chloride (Cl^{-}), nitrate (NO_3^{-}), sulfate (SO_4^{2-}) or phosphate (PO_4^{3-}). PFAS and these ions could have complex electrostatic interactions with these mineral ions and ultimately affect the membrane filtration performances [20]. Typically, elevated water salinity may trigger a shielding effect on the negatively charged membrane, leading to a reduction in the thickness of the electrical double layer. This decrease diminishes the electrostatic repulsion between the membrane and PFAS, consequently lowering the rejection rate [34].

Fig. 2 compares the rejection efficiencies of PFOA and PFBA by the RO and NF membranes when NaCl, $MgCl_2$, $AlCl_3$ Na_2SO_4 and Na_3PO_4 were added at the same molar concentration (100 mM). Tables S3 and S4 indicate that the spiked salts did not induce noticeable membrane scaling or reduction in permeate flux, which therefore is not a major factor for the PFAS removal. The dependence of the removal of PFOA and PFBA on the types of cation or anions is more evident for the NF membranes than for the RO membrane. Fig. 2a and b shows that varying the types of these ions did not change the rejection efficiencies of PFOA and PFBA by RO, since both PFOA and PFBA are larger than the membrane pores of RO and thus are effectively rejected regardless of the

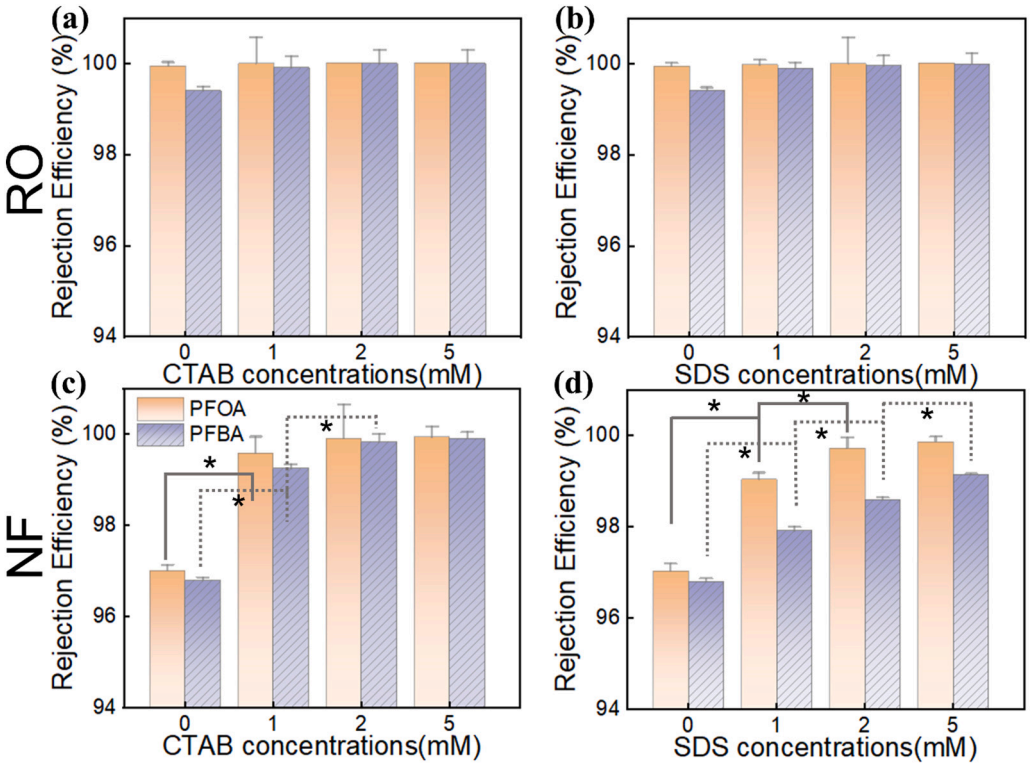

Fig. 1. Rejection efficiencies of PFOA and PFBA by the RO and NF membranes in the presence of CTAB (a)–(c) and SDS (b)–(d). * represents significant differences ($p < 0.05$) between two test groups. Operation condition: Temperature for all experiment was 25 °C, TMP of RO and NF was 55.0 bar and 13.8 bar, respectively.

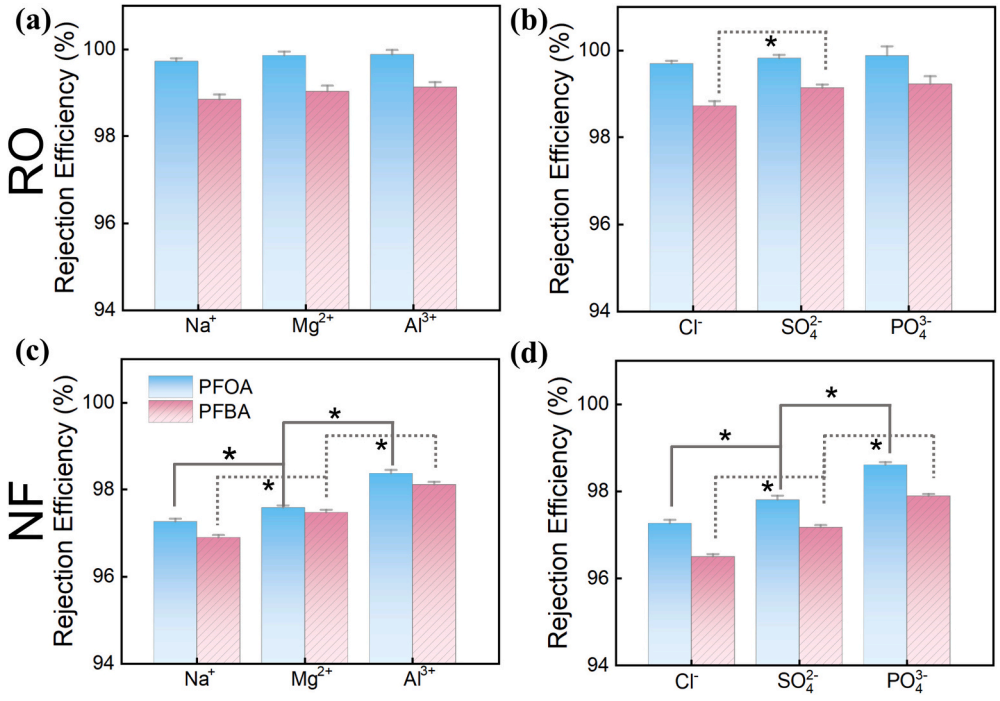

Fig. 2. Rejection efficiencies of PFOA and PFBA by the RO and NF membranes with different salts at 100 mM and pH around 5.6. (a) and (c) are the results when NaCl, $MgCl_2$ and $AlCl_3$ were present. (b) and (d) are the results when NaCl, Na_2SO_4 and Na_3PO_4 were present. * Represent significant differences ($p < 0.05$, *t*-test) between two test groups.

presence of different ions in the feed solution. Recent studies have questioned solution-diffusion model for describing the solvent transport in RO membrane and concluded that water and solvent transport in RO membranes is driven by a pressure gradient and solvent permeance depends on solvent viscosity, solvent molecular size and membrane pore size [35,36]. The presence of different salts in feed solution could significantly alter the membrane surface characteristics and the interactions with PFAS. Moreover, Fig. 2c and d indicates that under the

same operation condition, the rejection of both PFOA and PFBA by NF slightly increased when the ion valence increased from +1 to +3 or decreased from −1 to −3. This result is consistent with a study showing that Na^{+}, Ca^{2+}, and Fe^{3+} at same concentration of 0–2 mM escalated the rejection efficiency of PFOS (100 μg L^{-1} or 0.2 μM) by a NF (ESNA1-K1) membrane by 2–3 % due to the bridging interactions between polyvalent valence cations and group of PFOS molecules [20]. Positively charged cations could interact with the negatively charged PFAS and increase effective molecular size of PFAS via the formation of a PFAS-cation complex, which thus increased the rejection efficiency by RO or NF [22]. Thus, Al^{3+} exhibited the most pronounced impact on the rejection efficiency enlargement of PFOA and PFBA, probably because of the above complexation effect. Aside from differences in valence of cations or anions, the impact of ionic strength on PFAS rejection is also a critical factor. To date, there are few studies exploring the interplay between long- and short-chain PFAS, reverse osmosis (RO) and nanofiltration (NF) membranes, and the effects of ions and ionic strength. Our previous paper shows that high salinity of NaCl would cause the increase of the osmotic pressure and result in decline of PFOA/PFBA rejection [14]. Similarly, Wang et al. found that as the ionic strength of feed solutions increased from 0 to 100 mM NaCl, the rejection of PFBS dropped from 48.9 % to 20.5 %, whereas the rejection of PFOS only increased slightly from 89.6 % to 91.5 % [17]. This may be attributed to the difference in the size and electrostatic forces between the short-chain PFBS and the long-chain PFOS. The shorter-chain PFBS is easier to penetrate the NF membrane under the weak electrostatic repulsion and weak size exclusion mechanism. Conversely, Zhao et al. found that the presence of Ca^{2+} and Mg^{2+} enhanced the rejection of long-chain PFOS by the NF270 membrane [20], because multivalent cations could complex with PFAS and increase their molecular size, which ultimately results in greater rejection by the membrane.

Compared to Cl^{-} and SO_4^{2-}, PO_4^{3-} exhibited the most noticeable impact on the NF membrane rejection of PFOA and PFBA, as PO_4^{3-} tends to escalate electronegativity of NF membrane surface as supported by Fig. 3, which thus increased the PFOA and PFBA rejection [22]. The surface zeta potential data for both two membrane surfaces at different pH values and different salt concentrations under a fixed pH of 7 are shown in Fig. 3 and Table 1. Compared to the pristine RO and NF membrane surfaces, the surface zeta potential became lowered when the valence of the cations increased or when the cation concentration increased as the cations in the feed water could absorb on RO/NF membrane surface and thus reduce the negative charges or the zeta potentials. Table 1 shows there were greater negative surface zeta potentials for both two membranes when SO_4^{2-} and PO_4^{3-} were present, indicatives of the surface adsorption of these anions. The higher negative zeta potential will enhance the PFOA and PFBA rejection efficiency because of the reinforced electrostatic repulsion. Similar to cations ions, the membrane zeta potential gradually reduced as the anionic ion concentration increased, probably because of the compression of the Helmholtz double layer (e.g., diffuse layer). As a result, at higher ionic strength, the thinner diffuse layer could increase the tendency of the

Table 1
Zeta potentials of membrane surfaces with different salt concentrations under pH = 7.

Salts	Membrane	1 mM	10 mM	100 mM
NaCl	RO	−22.3 ± 1.0	−17.5 ± 1.5	−12.4 ± 1.3
	NF	−43.7 ± 1.1	−32.5 ± 1.3	−23.6 ± 1.4
$MgCl_2$	RO	−18.4 ± 1.3	−16.5 ± 1.2	−12.6 ± 1.4
	NF	−35.9 ± 0.7	−27.7 ± 0.8	−25.4 ± 1.7
$AlCl_3$	RO	−17.3 ± 1.1	−14.3 ± 0.9	−12.7 ± 1.2
	NF	−32.7 ± 2.1	−26.3 ± 1.8	−22.6 ± 1.0
Na_2SO_4	RO	−36.4 ± 2.6	−19.6 ± 1.0	−14.2 ± 1.1
	NF	−41.4 ± 2.9	−30.2 ± 1.8	−24.5 ± 2.1
Na_3PO_4	RO	−38.7 ± 2.3	−20.5 ± 1.7	−14.7 ± 1.0
	NF	−47.4 ± 3.1	−34.4 ± 2.1	−25.7 ± 1.5

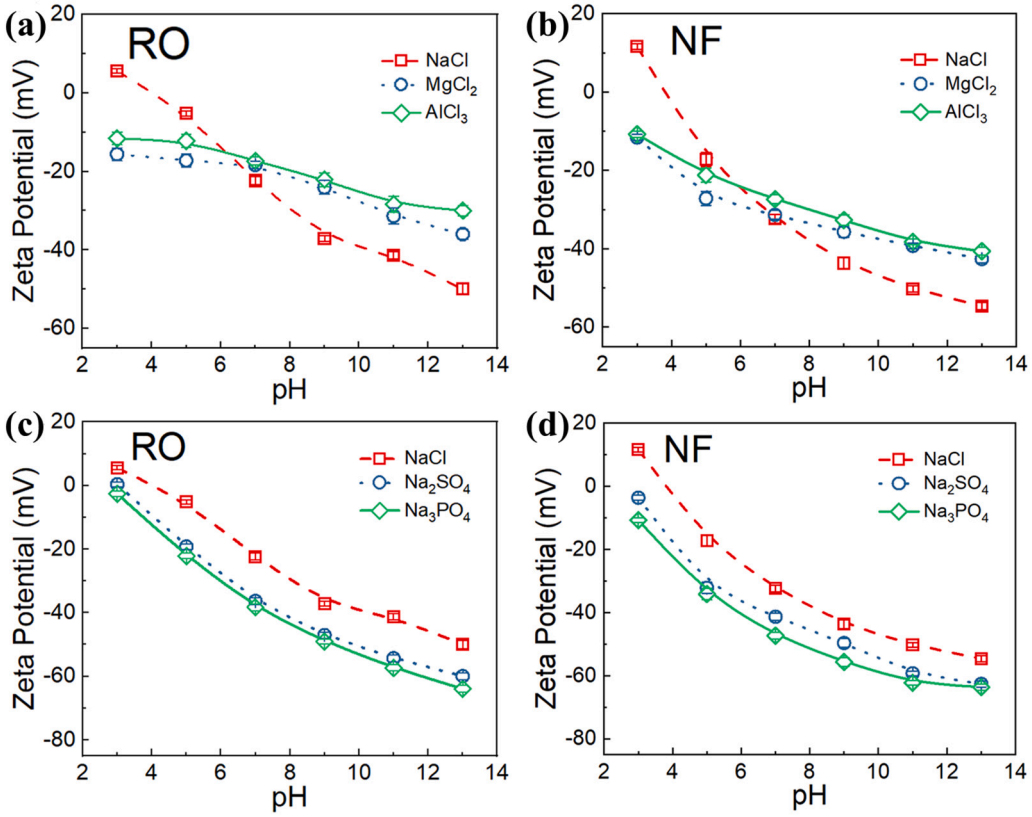

Fig. 3. The RO and NF membrane surface zeta potentials with 1 mM various salts (NaCl, Na_2SO_4, Na_3PO_4, $MgCl_2$, and $AlCl_3$) in DI water at different pHs.

PFAS adsorption and even passage across the membrane as reported previously [14,34].

3.3. Effects of operation temperature on rejections of PFOA and PFBA

Temperature can influence the performance of membrane-based filtration processes due to its effects on both the physical properties of the solution and the membrane itself [37,38]. For example, a higher solution temperature may cause thermal expansion of most polymeric membrane materials and decreased water viscosity and increased diffusion of solutes across the pores [39], which could potentially reduce the rejection of PFAS. Thus, we first measured the mean pore size of the NF membrane under different operation temperatures ranges from 15 to 45 °C as shown in Fig. 4a. Our result shows that the evaluated pore size of the tested NF membrane increased from 0.41 ± 0.04 nm at 15 °C to 0.65 ± 0.07 nm at 45 °C. The increased pore sizes of commercial NF membranes at high solution temperatures were reported previously [39,40]. The permeate flux of our tested NF membrane also increased from 75 LMH to 95 LMH when the solution temperature increased from 15 to 45 °C as shown in Fig. 4b, suggesting a pore opening or increase at high solution temperatures.

At elevated temperatures, the lower viscosity of water can improve overall membrane flux for both RO and NF membranes. However, no significantly different flux changes occurred to the RO membrane in our experiments under the solution temperature variations. Some previous studies reported a decline of water fluxes when the solution temperature decreased. For example, a polyamide composite RO membrane (flat sheet, XLE) was found to have a decreased flux as the solution temperature decreased from 35 to 15 °C when treating synthetic river water with the total dissolved solid content of 3.61 $g{\cdot}L^{-1}$ due to the scale formation [41]. Moreover, another study did not observe this the permeate flux variation for the same RO membrane under different temperatures (35, 25, and 15 °C) using 50 mM NaCl combined with 7.5 ppm humic acid solution as a feed. Instead, the permeate fluxes were similar at 25 and 35 °C, whereas the flux decline was only significant at 15 °C due to the increased fouling [42]. Our results shows the tested RO membrane yielded a stable water permeability in the temperature range (15 °C to 45 °C), suggesting that this temperature variation may not cause significant structural changes to the RO membrane. In addition, an increased permeate flux from 45.41 LMH to 57.87 LMH was observed when the solution temperature further increased from 45 °C to 70 °C (data are not shown in Fig. 4b), likely to due to the structural changes of the heated membrane or significantly reduction (~33 %) of water viscosity [43].

The rejection of PFBA by this NF membrane decreased substantially with the solution temperature increased from 15 to 45 °C compared to the result of PFOA (Fig. 4c). However, the rejection of PFOA did not substantially reduce when the solution temperature increased, probably because PFOA may have a larger molecular radius than PFBA. As shown in Fig. 4d, the rejection of PFOA and PFBA by the RO membrane followed a similar trend as the NF membrane. No significant change of PFOA rejection with the increased solution temperature. The PFBA rejection slightly decreased from 96.4 % to 95.1 % as temperature increased from 15 °C to 45 °C, which agrees with other studies [44]. For example, Dang et al. applied the pore-hindrance model to explain the expansion of a polyamide membrane's pore size by 13 % as the solution temperatures increased from 20 °C to 40 °C and the ultimate impact on solute diffusion and pollutant rejection [39].

In addition, we also analyzed the temperature dependence of the solute transport mechanisms. As the solution temperature rose from 15 to 45 °C, the diffusion coefficients of PFOA and PFBA increased significantly, as summarized in Table S3, which reduce the PFAS removal efficiency [39,45]. Table S4 also shows that PFBA had greater diffusion coefficients than PFOA at all four temperature and thus its diffusivity

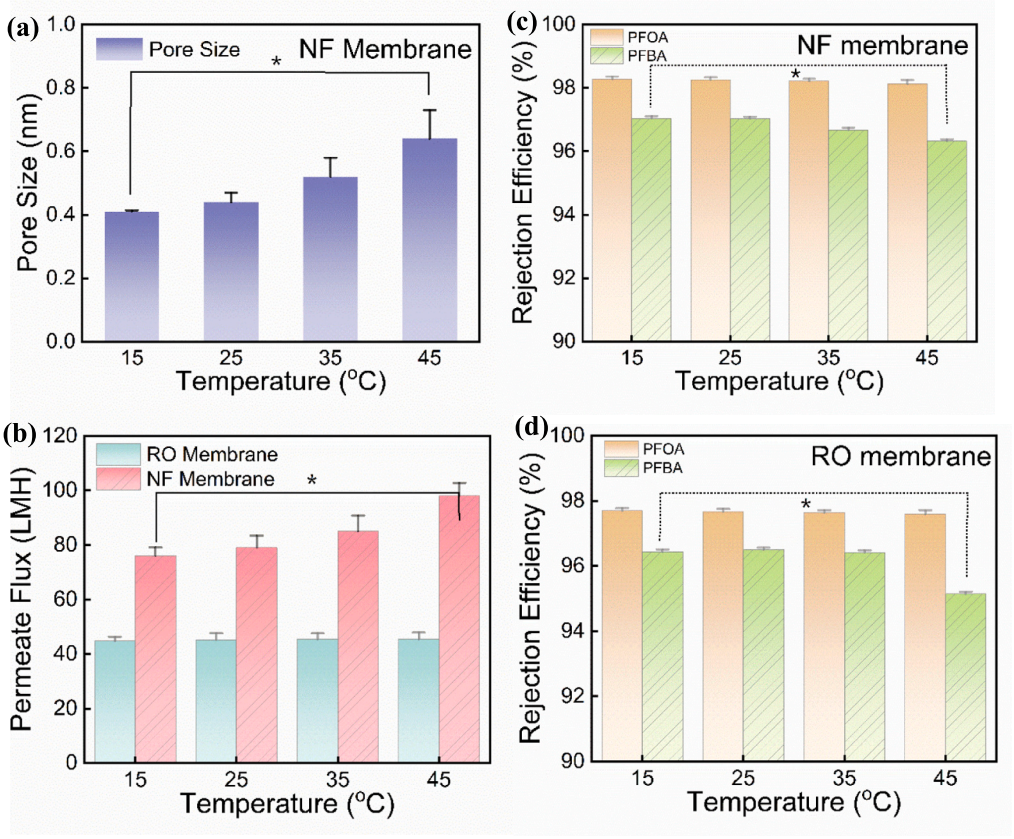

Fig. 4. (a) Pore radius changes of the NF membrane at different solution temperatures. (b) Permeate flux changes of the RO/NF membranes. (c)–(d) The rejection efficiencies of PFOA and PFBA by the NF and RO membranes at different temperatures. * represents significant differences ($p < 0.05$) between two test groups.

across the NF membrane was also greater, which explains rapid decline of rejection efficiency as the solution temperature rose. Moreover, the Knudsen number (K_n) was analyzed to reveal the temperature impact on transport mechanisms of solutes across the NF membrane. For both PFOA and PFBA, the K_n is larger than 1 (1.38–1.93 for PFOA and 2.01–2.82 for PFBA), which indicates the contribution of Knudsen diffusion to the mass transfer the two PFAS is significant as the characteristic length scale of the flow (the diameter of the nanopore) is small relative to the mean free path of the molecules being transported. The decrease in K_n with the increased temperature for PFAS implies that the increase of the membrane pore size outweighed the increased mean free path of PFAS molecules. For PFOA, the K_n value decrease to 1.38 at 45 °C indicates a possible transitioning from the rarefied regime to the continuum regime where transports phenomenon is governed bulk fluid properties. Finally, $D_{Effective}$ represents a weighted average of the bulk molecular diffusion coefficient and the Knudsen diffusion coefficient. For both PFAS, $D_{Kunsden}$ is larger than D_{bulk}, confirming that Knudsen diffusion is more significant during the NF membrane filtration.

3.4. Surface characterization of the pristine and used RO/NF membranes

3.4.1. Chemical mapping by AFM-IR

PFAS accumulation on filtration membrane surfaces may induce changes of membrane surface properties and interfere with PFAS rejection and water permeability. Chemical mapping of PFOA on both RO and NF membrane surfaces was achieved via AFM-IR on local membrane surfaces. Fig. 5 presents the typical results of AFM-IR mapping for the RO/NF membranes before and after filtration of PFOA in DI water without any surfactants or metal cations in a scale of 500 nm × 500 nm. The left column images compare the morphology of the four membrane samples. The IR mapping images in the middle column render the image contrast based on local thermal expansion of the membranes by applying the specific IR wavenumber of 1206 cm^{-1} that correspond to the asymmetric stretching of CF_2 and CF_3 bond [46]. Accordingly, the PFOA-deposited NF or RO membranes rendered more red areas than the pristine ones due to the higher abundance of $–CF_3$, which results in greater IR absorbance and thus the local thermal expansion as indicated by the greater amplitude of the positive tip deflection voltage.

Compared to the FTIR mapping, this AFM-IR technique clearly offers more sensitive and localized detection of PFOA on polymer membrane surface, which has not been reported. The IR spectra in the right column show that the PFOA-deposited membranes generated characteristic peaks of PFOA. Peaks at 1150 cm^{-1} represent the symmetric CF_2 stretch, peaks at 1200 cm^{-1} represent the asymmetric stretching of CF_2 and CF_3, peaks at 1250 cm^{-1} are an asymmetric CF_2 stretch and peaks at 1750 cm^{-1} indicate the carboxylate group (COOH). Both RO and NF membranes demonstrate the peaks due to C═O stretching (amide I at 1672 cm^{-1}) and N − H bending (amide II at 1544 cm^{-1}). The peaks at 1584, 1504, and 1488 cm^{-1}, were attributed to the aromatic ring C − C stretching motion. These peaks suggest the existence of polyamide in both RO and NF membranes.

3.4.2. Work function mapping by KPFM

The KPFM results in Fig. 6 show the topography and surface potential changes before and after filtration of the PFAS. The height images (a and b) indicate that the membrane surface morphology underwent minimal alteration. The CPD images (c and d) convey an increase in surface potential across the sample's topography for both RO and NF membranes. The right panels of Fig. 6 show the average difference in CPD for the pre-

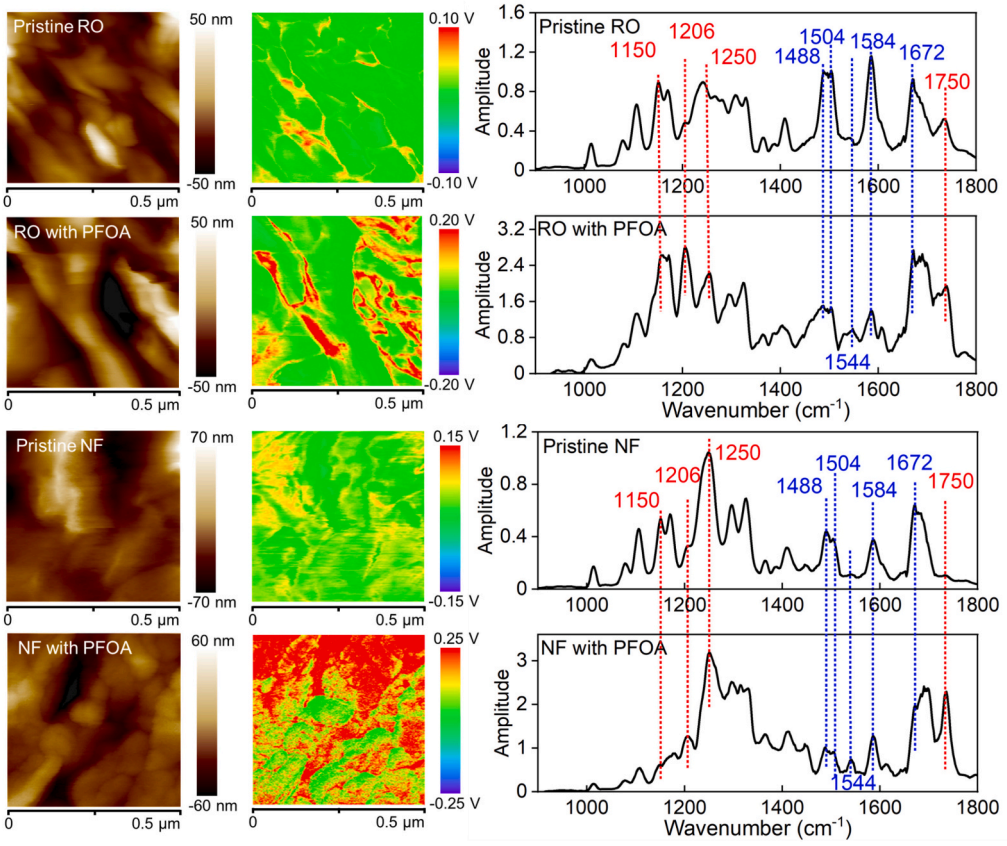

Fig. 5. The left two panels show the morphology and IR maps for the pristine and PFOA-deposited RO and NF membranes. The right panel shows the IR spectra of the membranes that indicates the presence of the PFOA absorbance at 1206 cm^{-1}. Operation condition: Temperature for all experiment was 25 °C, PFOA or PFBA concentration was 10 mg·L^{-1}, TMP of RO and NF was 55.0 bar and 13.8 bar, respectively.

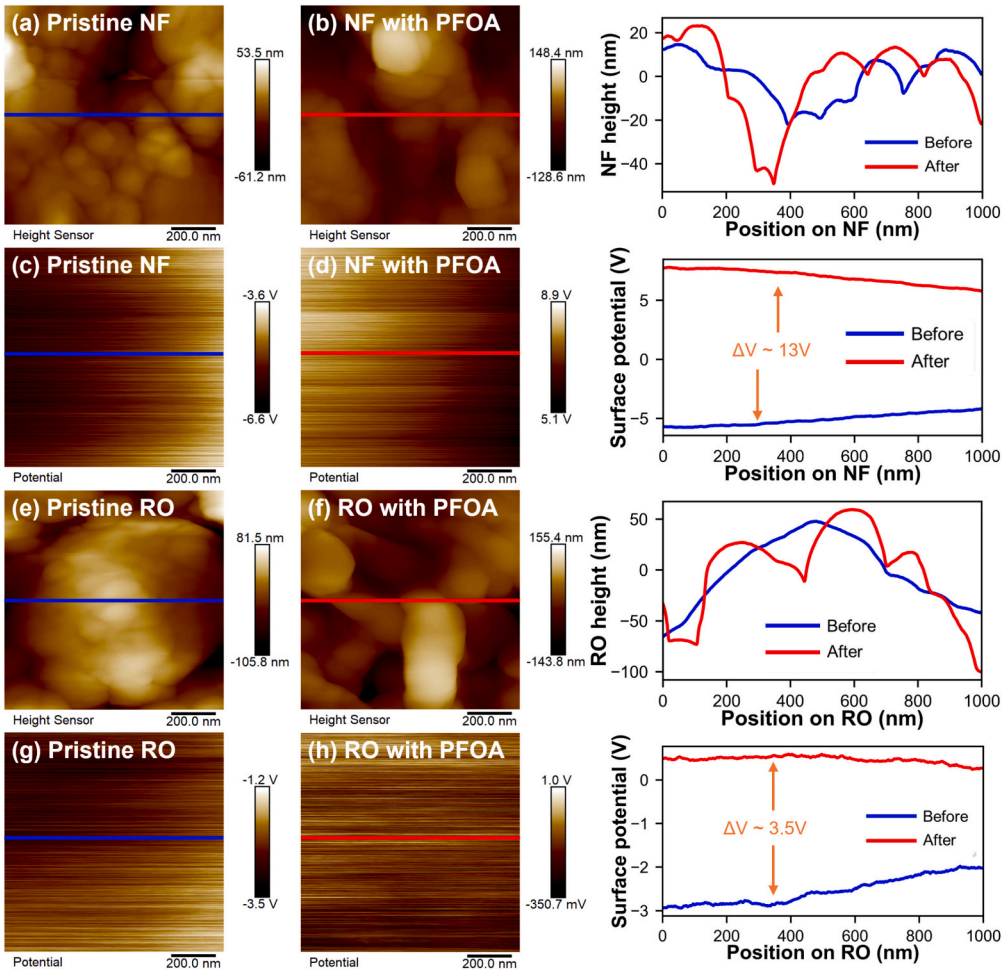

Fig. 6. High-resolution images of the topography (a–b) and surface potential (c–d) of the pristine NF membrane and the used NF membrane after PFAS filtration. The right panel shows the difference in topography and CPD signal (surface potential).

and post-filtration of PFOA are ~13 V and ~ 3.5 V, respectively, for the NF and RO membranes. The work function of the pristine and used RO membranes increased from 2.82 eV to 5.53 eV as calculated by Eq. (S1). For the NF membrane, it increased from 0.04 eV to 12.25 eV. Thus, the elevated work function at the membrane surface suggests the PFAS adsorption increased the energy necessary for electrons to overcome the potential barrier and escape from the surface of the membrane. The presence of the -CF_3 group in PFOA generally imparts enhanced electronegativity to the membrane's surface and increased the surface work function. Additional KPFM tests on a PFOA-adsorbed silicon wafer surface (the bright region in Fig. S2) reveal the dried-up PFOA molecules form a meticulous arrangement of crystal-like structures with a layer thickness of a few nanometers. Moreover, there is a steep positive shift in surface potential of ~250 mV compared to the surface without PFOA (the dark region). These observational results are corroborated by Bai et al. (2021), who confirmed that the surface potential of graphite exposed to ambient conditions can be affected by surface contaminations [47]. This KPFM result further supports the observation of AFM-IR that the presence of PFAS on the membrane surface altered both chemical fingerprints but also electronic properties of the polymeric RO/NF membranes.

4. Conclusion

This comprehensive study sheds light on the intricate influences of operating temperature, two surfactants, and ion valency on PFAS removal using commercial RO and NF membranes, which remain largely elusive but crucial for enhancing our understanding of membrane separation of PFAS. The presence of SDS and CTAB surfactants didn't show any noticeable impacts on PFOA and PFBA rejections on RO, while they both enhanced the PFOA and PFBA rejection (2–3 %) with NF. The RO membranes maintained high rejection of PFOA and PFBA with the change of coexistence cationic (Na^+, Mg^{2+}, and Al^{3+}) or anionic ions (Cl^-, SO_4^{2-}, and PO_4^{3-}), likely the rejection mechanism of RO for PFAS is primarily size exclusion. The variation of cationic and anionic ions was found to enhance the rejection efficiency of PFOA and PFBA with NF membrane by 2–3 %. Temperature induced pore size change of NF membrane and diffusivity variation of PFAS molecules could play a role in enhancing/reducing the removal efficiency of PFBA and PFOA. Increased temperature causing larger mean free path of the PFAS molecules lead to intense molecular-membrane wall collisions and significant Knudsen diffusion (K_n range: 1.38–1.93 for PFOA and 2.01–2.82 for PFBA) during filtration processes. Additionally, AFM-IR technique allows for the nanoscale-detection of PFOA surface adsorption on membranes at remarkably low levels through the wavelengths of 1206 cm^{-1}(-CF_3) and 1705 cm^{-1} (-COOH). Chemical mapping at 1206 cm^{-1} indicates the higher signal after PFOA filtration for both NF and RO. The introduction of KPFM technique also shows the ability to detect tracing-level PFOA surface adsorption by the difference in work function of membrane between pre- and post PFOA filtration (~13 V for NF and ~ 3.5 V for RO).

CRediT authorship contribution statement

Qingquan Ma: Writing – review & editing, Writing – original draft, Visualization, Investigation, Formal analysis, Data curation. **Jiahe Zhang:** Writing – original draft, Visualization, Formal analysis, Data curation. **Guangyu Zhu:** Writing – original draft, Formal analysis, Data curation. **Neel Ahuja:** Writing – original draft, Formal analysis. **Boris Khusid:** Writing – review & editing, Supervision. **Wen Zhang:** Writing – review & editing, Supervision, Project administration.

Declaration of competing interest

The authors declare that they have no conflict of Interest.

Data availability

Data will be made available on request.

Acknowledgement

This research was carried out in the NSF Industry/University Cooperative Research Center for Membrane Science, Engineering and Technology that has been supported by the NSF Award IIP-1822130. The authors want to thank the constructive feedback from the project mentors, Uwe Beuscher from W.L. Gore & Associates, Inc. and Albert Wu from 3M as well as support from the MAST center's industrial advisory board (IAB) members.

Appendix A. Supplementary data

AFM-IR and KPFM operation details, surfactants impacts on PFOA and PFBA rejection, and surface zeta potential data. Supplementary data to this article can be found online at https://doi.org/10.1016/j.jwpe.2024.106039.

References

[1] S. Kurwadkar, J. Dane, S.R. Kanel, M.N. Nadagouda, R.W. Cawdrey, B. Ambade, G. C. Struckhoff, R. Wilkin, Per-and polyfluoroalkyl substances in water and wastewater: a critical review of their global occurrence and distribution, Sci. Total Environ. 809 (2022) 151003.
[2] B. Ji, Y. Zhao, Y. Yang, Q. Li, Y. Man, Y. Dai, J. Fu, T. Wei, Y. Tai, X. Zhang, Curbing per-and polyfluoroalkyl substances (PFASs): first investigation in a constructed wetland-microbial fuel cell system, Water Res. 230 (2023) 119530.
[3] V. Franke, M. Ullberg, P. McCleaf, M. Wålinder, S.J. Köhler, L. Ahrens, The price of really clean water: combining nanofiltration with granular activated carbon and anion exchange resins for the removal of per-and polyfluoroalkyl substances (PFASs) in drinking water production, ACS ES&T Water 1 (4) (2021) 782–795.
[4] N. Bolan, B. Sarkar, Y. Yan, Q. Li, H. Wijesekara, K. Kannan, D.C. Tsang, M. Schauerte, J. Bosch, H. Noll, Remediation of poly-and perfluoroalkyl substances (PFAS) contaminated soils–to mobilize or to immobilize or to degrade? J. Hazard. Mater. 401 (2021) 123892.
[5] M. Park, S. Wu, I.J. Lopez, J.Y. Chang, T. Karanfil, S.A. Snyder, Adsorption of perfluoroalkyl substances (PFAS) in groundwater by granular activated carbons: roles of hydrophobicity of PFAS and carbon characteristics, Water Res. 170 (2020) 115364.
[6] M. Riegel, B. Haist-Gulde, F. Sacher, Sorptive removal of short-chain perfluoroalkyl substances (PFAS) during drinking water treatment using activated carbon and anion exchanger, Environ. Sci. Eur. 35 (1) (2023) 1–12.
[7] M. Sun, E. Arevalo, M. Strynar, A. Lindstrom, M. Richardson, B. Kearns, A. Pickett, C. Smith, D.R.U. Knappe, Legacy and emerging perfluoroalkyl substances are important drinking water contaminants in the cape fear river watershed of North Carolina, Environ. Sci. Technol. Lett. 3 (12) (2016) 415–419.
[8] P. McCleaf, S. Englund, A. Östlund, K. Lindegren, K. Wiberg, L. Ahrens, Removal efficiency of multiple poly- and perfluoroalkyl substances (PFASs) in drinking water using granular activated carbon (GAC) and anion exchange (AE) column tests, Water Res. 120 (2017) 77–87.
[9] M.F. Rahman, S. Peldszus, W.B. Anderson, Behaviour and fate of perfluoroalkyl and polyfluoroalkyl substances (PFASs) in drinking water treatment: a review, Water Res. 50 (2014) 318–340.
[10] S. Senevirathna, S. Tanaka, S. Fujii, C. Kunacheva, H. Harada, B.R. Shivakoti, R. Okamoto, A comparative study of adsorption of perfluorooctane sulfonate (PFOS) onto granular activated carbon, ion-exchange polymers and non-ion-exchange polymers, Chemosphere 80 (6) (2010) 647–651.
[11] D. Li, K. Londhe, K. Chi, C.S. Lee, A.K. Venkatesan, B.S. Hsiao, Functionalized bio-adsorbents for removal of perfluoroalkyl substances: a perspective, AWWA Water Science 3 (6) (2021) e1258.
[12] S.J. Chow, H.C. Croll, N. Ojeda, J. Klamerus, R. Capelle, J. Oppenheimer, J. G. Jacangelo, K.J. Schwab, C. Prasse, Comparative investigation of PFAS adsorption onto activated carbon and anion exchange resins during long-term operation of a pilot treatment plant, Water Res. 226 (2022) 119198.
[13] Y. Gao, S. Deng, Z. Du, K. Liu, G. Yu, Adsorptive removal of emerging polyfluoroalky substances F-53B and PFOS by anion-exchange resin: a comparative study, J. Hazard. Mater. 323 (2017) 550–557.
[14] Q. Ma, Q. Lei, F. Liu, Z. Song, B. Khusid, W. Zhang, Evaluation of commercial nanofiltration and reverse osmosis membrane filtration to remove per-and polyfluoroalkyl substances (PFAS): effects of transmembrane pressures and water matrices, Water Environment Research: a research publication of the Water Environment Federation 96 (2) (2024) e10983.
[15] C. Zeng, S. Tanaka, Y. Suzuki, S. Fujii, Impact of feed water pH and membrane material on nanofiltration of perfluorohexanoic acid in aqueous solution, Chemosphere 183 (2017) 599–604.
[16] H. Hara-Yamamura, K. Inoue, T. Matsumoto, R. Honda, K. Ninomiya, H. Yamamura, Rejection of perfluorooctanoic acid (PFOA) and perfluorooctane sulfonate (PFOS) by severely chlorine damaged RO membranes with different salt rejection ratios, Chem. Eng. J. 446 (2022) 137398.
[17] J. Wang, L. Wang, C. Xu, R. Zhi, R. Miao, T. Liang, X. Yue, Y. Lv, T. Liu, Perfluorooctane sulfonate and perfluorobutane sulfonate removal from water by nanofiltration membrane: the roles of solute concentration, ionic strength, and macromolecular organic foulants, Chem. Eng. J. 332 (2018) 787–797.
[18] C. Zhao, C.Y. Tang, P. Li, P. Adrian, G. Hu, Perfluorooctane sulfonate removal by nanofiltration membrane—the effect and interaction of magnesium ion/humic acid, J. Membr. Sci. 503 (2016) 31–41.
[19] C. Zhao, J. Zhang, G. He, T. Wang, D. Hou, Z. Luan, Perfluorooctane sulfonate removal by nanofiltration membrane the role of calcium ions, Chem. Eng. J. 233 (2013) 224–232.
[20] C. Zhao, G. Hu, D. Hou, L. Yu, Y. Zhao, J. Wang, A. Cao, Y. Zhai, Study on the effects of cations and anions on the removal of perfluorooctane sulphonate by nanofiltration membrane, Sep. Purif. Technol. 202 (2018) 385–396.
[21] Á. Soriano, D. Gorri, A. Urtiaga, Efficient treatment of perfluorohexanoic acid by nanofiltration followed by electrochemical degradation of the NF concentrate, Water Res. 112 (2017) 147–156.
[22] Q. Luo, Y. Liu, G. Liu, C. Zhao, Preparation, characterization and performance of poly (m-phenylene isophthalamide)/organically modified montmorillonite nanocomposite membranes in removal of perfluorooctane sulfonate, J. Environ. Sci. 46 (2016) 126–133.
[23] T. Jin, M. Peydayesh, R. Mezzenga, Membrane-based technologies for per-and poly-fluoroalkyl substances (PFASs) removal from water: removal mechanisms, applications, challenges and perspectives, Environ. Int. 157 (2021) 106876.
[24] S. Koner, A. Pal, A. Adak, Cationic surfactant adsorption on silica gel and its application for wastewater treatment, Desalin. Water Treat. 22 (1–3) (2010) 1–8.
[25] R. Li, O.F. Isowamwen, K.C. Ross, T.M. Holsen, S.M. Thagard, PFAS–CTAB complexation and its role on the removal of PFAS from a lab-prepared water and a reverse osmosis reject water using a plasma reactor, Environ. Sci. Technol. 57 (34) (2023) 12901–12910.
[26] F. Wang, Z.-Z. Jia, S.-J. Luo, S.-F. Fu, L. Wang, X.-S. Shi, C.-S. Wang, R.-B. Guo, Effects of different anionic surfactants on methane hydrate formation, Chem. Eng. Sci. 137 (2015) 896–903.
[27] B. Tah, P. Pal, M. Mahato, G. Talapatra, Aggregation behavior of SDS/CTAB catanionic surfactant mixture in aqueous solution and at the air/water interface, J. Phys. Chem. B 115 (26) (2011) 8493–8499.
[28] P. McCleaf, W. Stefansson, L. Ahrens, Drinking water nanofiltration with concentrate foam fractionation—a novel approach for removal of per-and polyfluoroalkyl substances (PFAS), Water Res. 232 (2023) 119688.
[29] X. Hang, X. Chen, J. Luo, W. Cao, Y. Wan, Removal and recovery of perfluorooctanoate from wastewater by nanofiltration, Sep. Purif. Technol. 145 (2015) 120–129.
[30] S. Das, A. Ronen, A review on removal and destruction of per-and polyfluoroalkyl substances (PFAS) by novel membranes, Membranes 12 (7) (2022) 662.
[31] Q. Ma, J. Gao, B. Moussa, J. Young, M. Zhao, W. Zhang, Electrosorption, desorption, and oxidation of perfluoroalkyl carboxylic acids (PFCAs) via MXene-based electrocatalytic membranes, ACS Appl. Mater. Interfaces. 15 (24) (2023) 29149–29159.
[32] Q. Ma, J. Young, S. Basuray, G. Cheng, J. Gao, N. Yao, W. Zhang, Elucidating facet dependent electronic and electrochemical properties of Cu2O nanocrystals using AFM/SCEM and DFT, Nano Today 45 (2022).
[33] A. Soon, M. Todorova, B. Delley, C. Stampfl, Thermodynamic stability and structure of copper oxide surfaces: a first-principles investigation, Phys. Rev. B 75 (12) (2007).
[34] C. Liu, X. Zhao, A.F. Faria, K.Y.D. Quiñones, C. Zhang, Q. He, J. Ma, Y. Shen, Y. Zhi, Evaluating the efficiency of nanofiltration and reverse osmosis membrane processes for the removal of per-and polyfluoroalkyl substances from water: a critical review, Sep. Purif. Technol. 302 (2022) 1, 122161.
[35] J. He, H. Fan, M. Elimelech, Y. Li, Molecular simulations of organic solvent transport in dense polymer membranes: solution-diffusion or pore-flow mechanism? J. Membr. Sci. 708 (2024) 123055.
[36] L. Wang, J. He, M. Heiranian, H. Fan, L. Song, Y. Li, M. Elimelech, Water transport in reverse osmosis membranes is governed by pore flow, not a solution-diffusion mechanism. Science, Advances 9 (15) (2023) eadf8488.

[37] Mei Qun Seah, Siew Fen Chua, Wei Lun Ang, Woei Jye Lau, Amir Mansourizadeh, Chidambaram Thamaraiselvan, Advancements in polymeric membranes for challenging water filtration environments: a comprehensive review, J. Environ. Chem. Eng. (2024) 112628.
[38] Y. Roy, D.M. Warsinger, Effect of temperature on ion transport in nanofiltration membranes: diffusion, convection and electromigration, Desalination 420 (2017) 241–257.
[39] H.Q. Dang, W.E. Price, L.D. Nghiem, The effects of feed solution temperature on pore size and trace organic contaminant rejection by the nanofiltration membrane NF270, Sep. Purif. Technol. 125 (2014) 43–51.
[40] B. Xu, W. Gao, B. Liao, H. Bai, Y. Qiao, W. Turek, A review of temperature effects on membrane filtration, Membranes 14 (1) (2023) 5.
[41] A. Jawor, E.M.V. Hoek, Effects of feed water temperature on inorganic fouling of brackish water RO membranes, Desalination 235 (1) (2009) 44–57.
[42] X. Jin, A. Jawor, S. Kim, E.M.V. Hoek, Effects of feed water temperature on separation performance and organic fouling of brackish water RO membranes, Desalination 239 (1) (2009) 346–359.
[43] L. Korson, W. Drost-Hansen, F.J. Millero, Viscosity of water at various temperatures, J. Phys. Chem. 73 (1) (1969) 34–39.
[44] X. Chen, A. Vanangamudi, J. Wang, J. Jegatheesan, V. Mishra, R. Sharma, S. R. Gray, J. Kujawa, W. Kujawski, F. Wicaksana, Direct contact membrane distillation for effective concentration of perfluoroalkyl substances–impact of surface fouling and material stability, Water Res. 182 (2020) 116010.
[45] R. Xu, M. Zhou, H. Wang, X. Wang, X. Wen, Influences of temperature on the retention of PPCPs by nanofiltration membranes: experiments and modeling assessment, J. Membr. Sci. 599 (2020) 117817.
[46] X. Gao, J. Chorover, Adsorption of perfluorooctanoic acid and perfluorooctanesulfonic acid to iron oxide surfaces as studied by flow-through ATR-FTIR spectroscopy, Environ. Chem. 9 (2) (2012) 148–157.
[47] R. Bai, N.L. Tolman, Z. Peng, H. Liu, Influence of atmospheric contaminants on the work function of graphite, Langmuir 39 (34) (2023) 12159–12165.